1 Spin structure factor

Our experiment measures the bulk spin structure factor $\bar{S}_{\boldsymbol{Q}}$ for an inhomogeneous realization of the Hubbard model. Theoretical approaches such as QMC and NLCE consider a homogeneous system with a finite number of lattice sites L^3 and calculate the structure factor

$$S_{\boldsymbol{Q}} = \frac{4}{L^3} \sum_{i,j} e^{i\boldsymbol{Q}\cdot(\boldsymbol{R}_i - \boldsymbol{R}_j)} \langle \sigma_{zi} \sigma_{zj} \rangle \tag{1}$$

In the local density approximation we can think of every point $\boldsymbol{r}$ of our lattice site as a homogeneous system for which $S_{\boldsymbol{Q}}(\boldsymbol{r})$ can be obtained. We can relate the measured bulk spin structure factor to the local $S_{\boldsymbol{Q}}(\boldsymbol{r})$ as

$$\bar{S}_{\boldsymbol{Q}} = \frac{1}{N} \int S_{\boldsymbol{Q}}(\boldsymbol{r}) \, \mathrm{d}^3\boldsymbol{r} \tag{2}$$

The NLCE data provided by Ehsan gives $S_{\boldsymbol{Q}}$ directly whereas the QMC data provided by Thereza gives $S_{\boldsymbol{Q}}/n$. To compare with experiment we have decided to use $S_{\boldsymbol{Q}}/n$ such that

$$\bar{S}_{\boldsymbol{Q}} = \frac{1}{N} \int \left[\frac{S_{\boldsymbol{Q}}}{n} \right]_{\boldsymbol{r}} n(\boldsymbol{r}) \, \mathrm{d}^3\boldsymbol{r} \tag{3}$$

Also, in our LDA calculations we have assumed that there is spherical symmetry in the system so

$$\bar{S}_{\boldsymbol{Q}} = \frac{4\pi}{N} \int \left[\frac{S_{\boldsymbol{Q}}}{n} \right]_{r_d} n(r_d) \; r_d^2 \, \mathrm{d}r_d \tag{4}$$

where r_d is the distance from the origin along a 111 body diagonal of the lattice.

The validity of the spherical symmetry assumption is very questionable, since away from the diagonal the lattice depths are different along the x, y, z directions and an anisotropic Hubbard model should be used. However, for simplicity this is how we decided to treat the system.

1.1 Effective fraction

In the current version of the paper we say something along the lines of : "x percent of the cloud contributes effectively to the observed structure factor". More formally x, the effective fraction is defined as

$$\bar{S}_{\boldsymbol{\pi}} - 1 = \frac{x}{100} \left([S_{\boldsymbol{\pi}}]_{\max} - 1 \right) \tag{5}$$

where $[S_{\boldsymbol{\pi}}]_{\max}$ is the maximum value attained by $S_{\boldsymbol{\pi}}(r_d)$.

We will see later on that the current LDA results (which are still not cold enough to match the experimental data) lead to an effective fraction of 40%. So, for our observed $\bar{S}_{\boldsymbol{\pi}} = 1.9$ then $[S_\pi]_{\max} = 3.3$, which would imply that the lowest local T/T_N in our cloud is $T/T_N \approx 1.5$ according to QMC calculations by Thereza, cf. Fig. 1.

So at the moment the best claim we can make is $T/T_N < 1.5$.

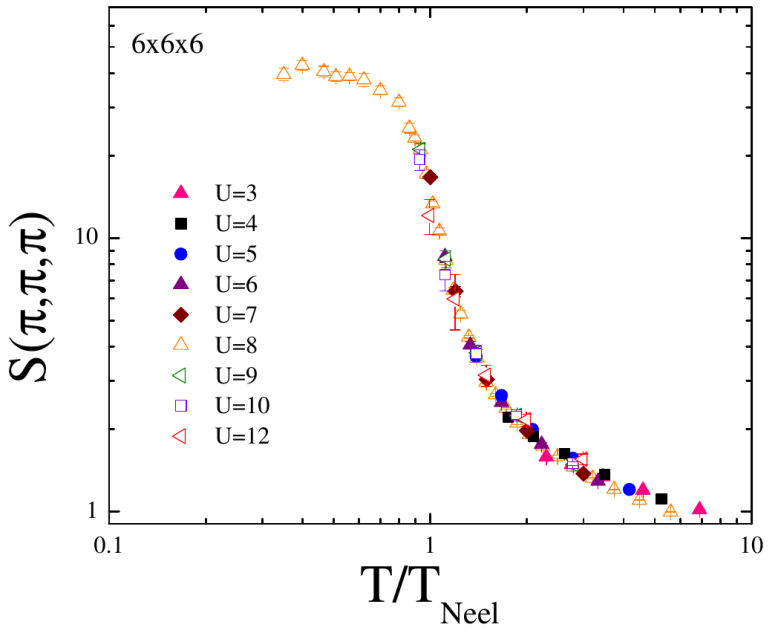

Figure 1: S_π vs T/T_N.

2 NLCE data

Ehsan has provided us with exact NLCE (numerical linked-cluster expansion) data down to $T/t = 1.6$. Below this temperature he can do a resummation to obtain the thermodynamic quantities. At values of the temperature around $T/t = 0.4$ the results start getting very noisy, however we can recover a usable data set by applying a low pass filter to the data[1]. The original data and the filtered data are shown in Fig. 2. Larger T/t values are less noisy, but the filter is still used up to $T/t = 1.4$ to remove some spurious points that show up in the data. At $T/t > 1.6$ the data is exact and it has no spurious points.

We can use the NLCE data to see that the density as a function of chemical potential is pretty much frozen for $T/t < 1.0$, see Fig. 3. The high temperature series expansion (HTSE) that I was using before to calculate density profiles works down to about $T/t \approx 1.6$, so I was unable to capture the "Mottness" of the density profile as we see it in the experiment.

The data for $S_{\boldsymbol{\pi}}/n$ provided by NLCE is shown in Fig. 4. Notice that to avoid errors when dividing by a small value of n we have decided to enforce $S_{\boldsymbol{\pi}} = 1$ for densities less than a density cutoff. The density cutoff is adjusted for each value of U/t.

3 QMC data

The QMC data does not suffer from noise problems for small values of T/t, however there is much less of it available. Fig. 5 shows the available U/t and T/t values. The entropy and double occupancy, not shown in the Figure are also available from Thereza's data set, as well as the structure factor in the $\boldsymbol{\theta}$ direction.

[1]The type of filter used is the Savitzky-Golay filter `http://www.wire.tu-bs.de/OLDWEB/mameyer/cmr/savgol.pdf`

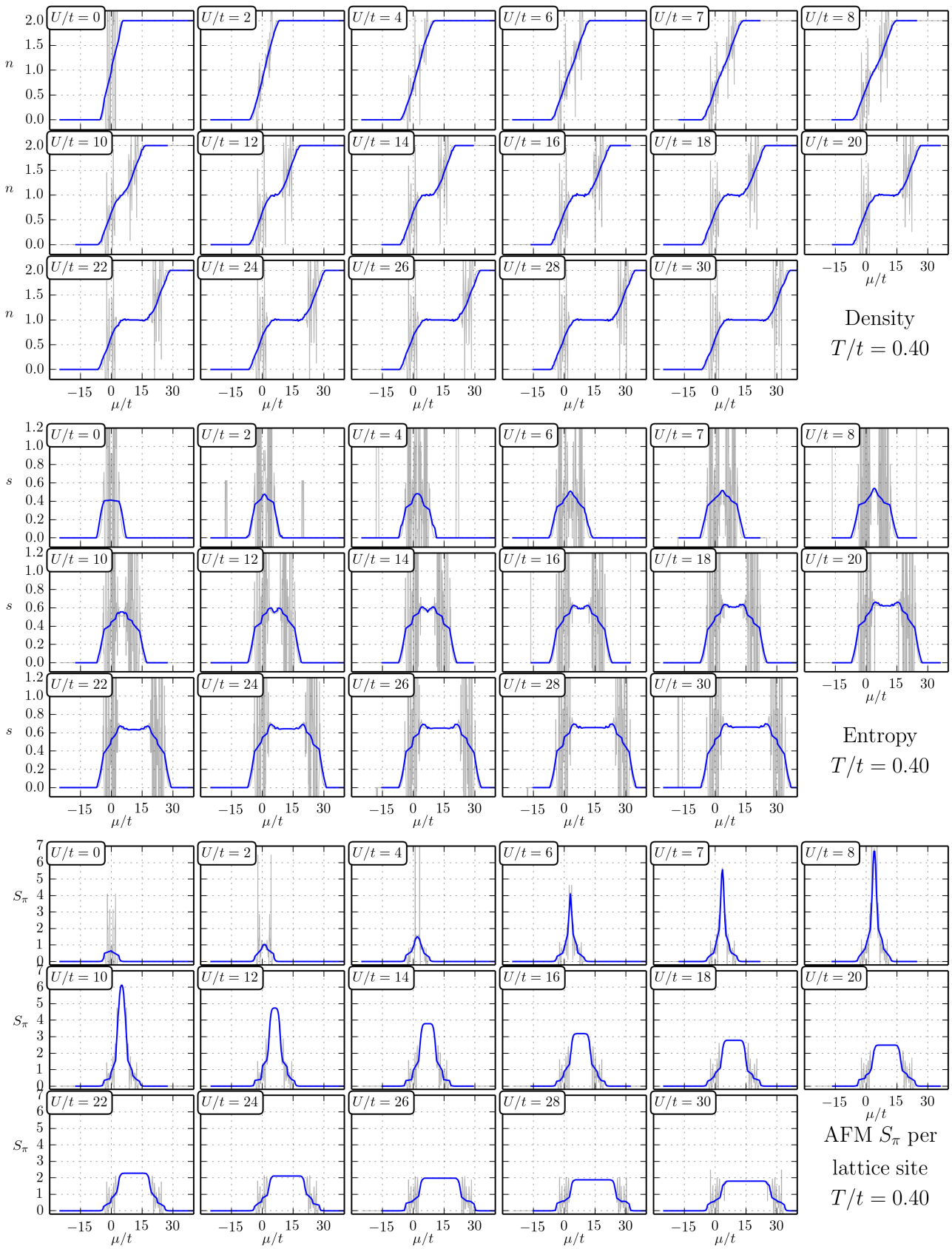

Figure 2: Lowest temperature data accessible to the NLCE by extrapolation, $T/t = 0.4$. The original data provided by Ehsan is shown in gray and the data after filtering is shown in blue.

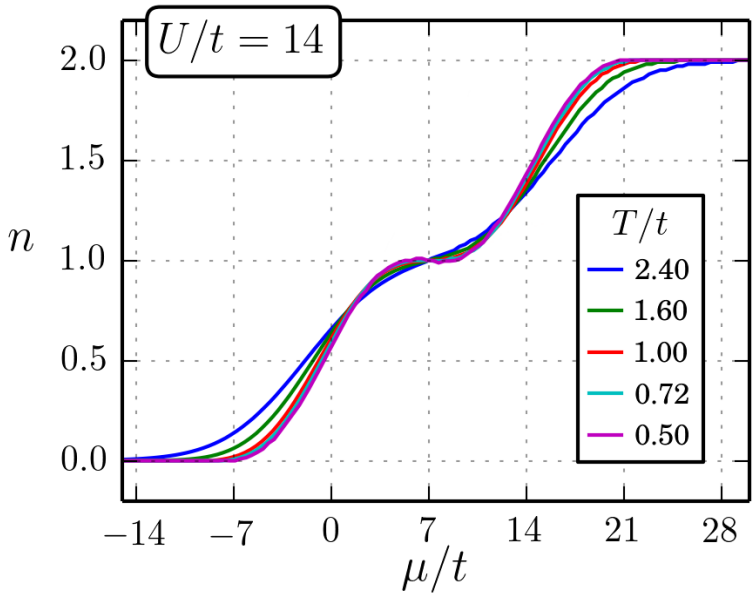

Figure 3: NLCE data at $U/t = 14$. For $T/t \leq 1$ the density does not shown much variation.

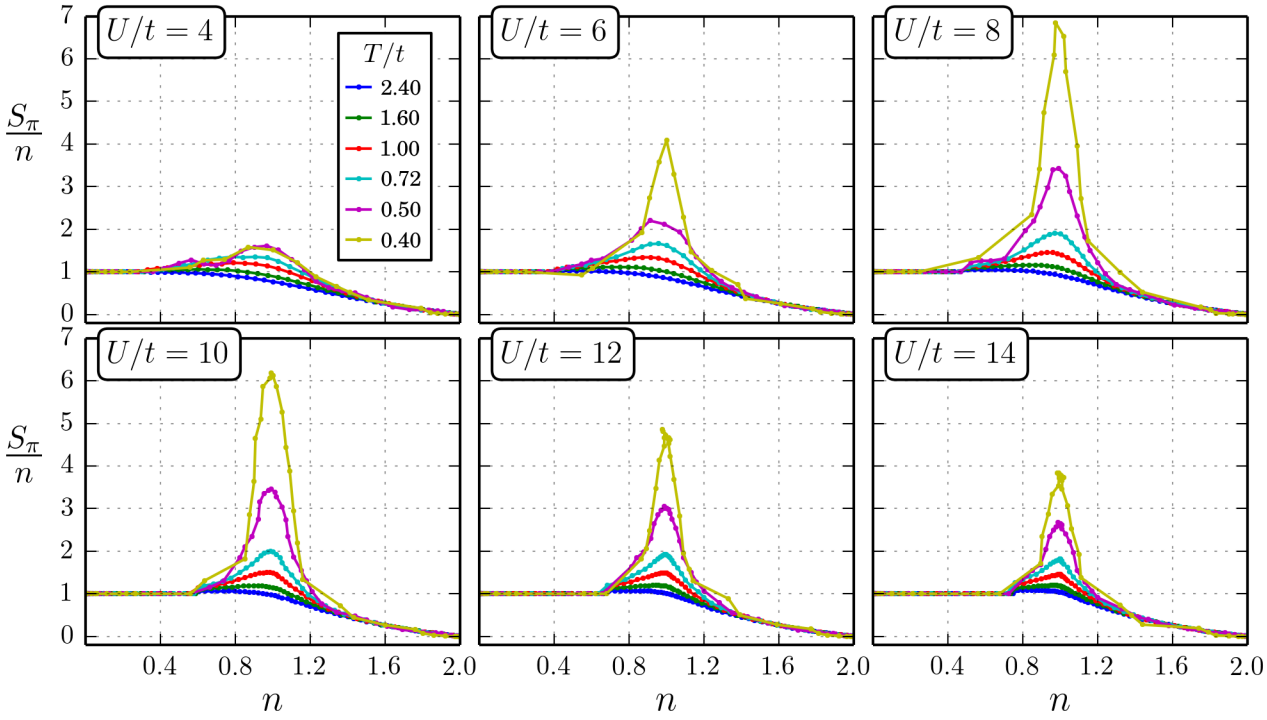

Figure 4: NLCE S_π/n data for various interactions and temperatures.

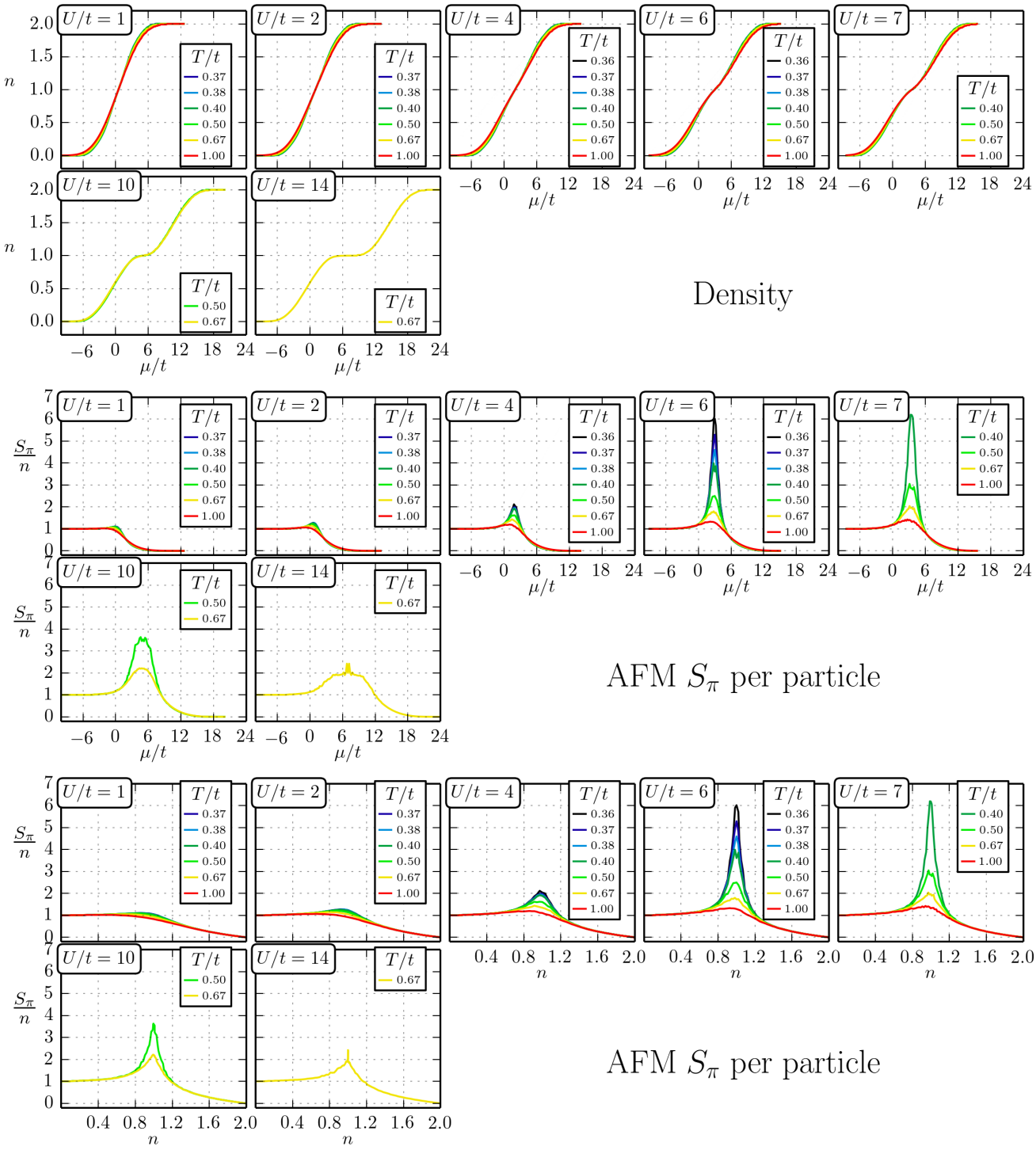

Figure 5: All available QMC data for the density, $S_{\boldsymbol{\pi}}$ and $S_{\boldsymbol{\pi}}/n$. Entropy, double occupancy and S_θ/n are available but not shown here.

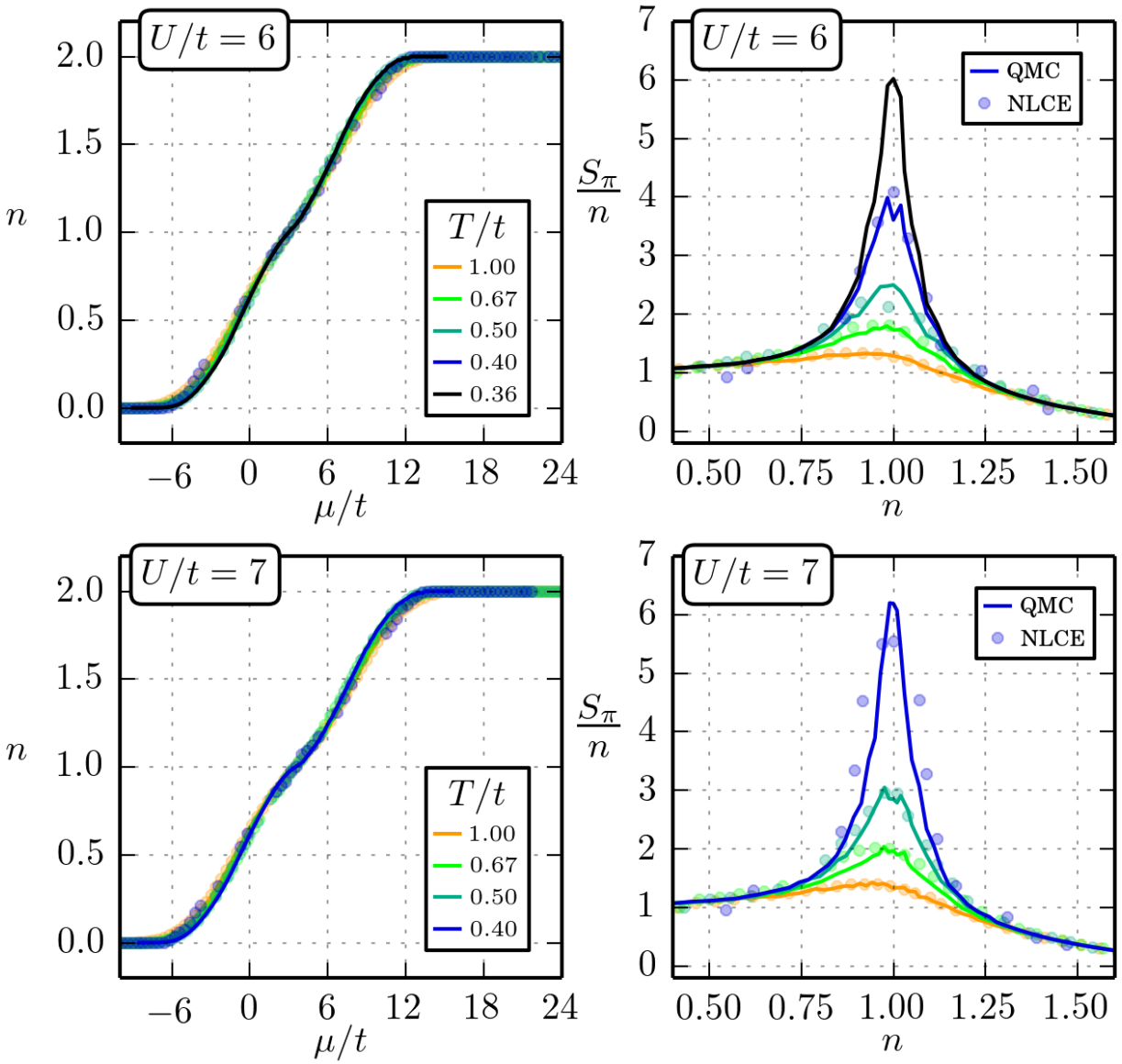

Figure 6: Comparison between QMC and NLCE data. At $U/t = 6$ both methods have data available whereas the QMC data at $U/t = 7$ is compared with the NLCE data at $U/t = 8$.

4 NLCE data and QMC data comparison

In Fig. 6 we show QMC and NLCE data sets on the same plot. A direct comparison is possible at $U/t = 6$. The QMC data at $U/t = 7$ is compared with NLCE at $U/t = 8$ which reveals that the NLCE structure factor is perhaps too broad as a function of n. It is clear from this plots that the density is frozen for $T/t < 1.0$ and that both QMC and NLCE have very good agreement on the density.

5 Comparison of experimental data with LDA

The way we will proceed is as follows:

1. Set up a trap geometry based on our experimental calibration. The trap geometry determines the

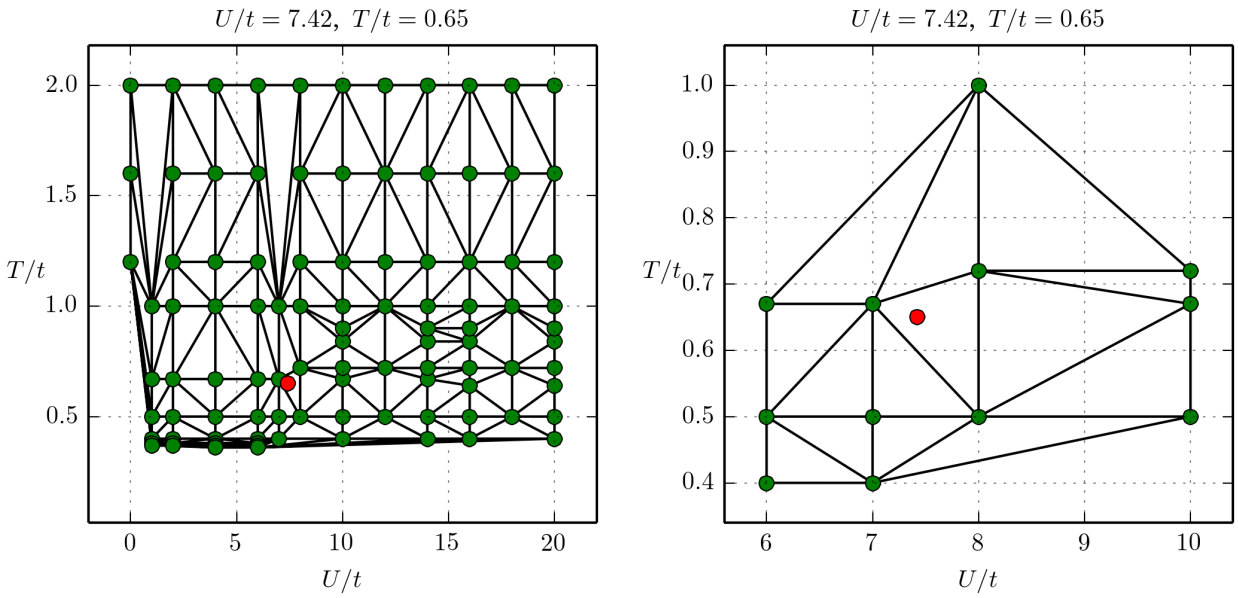

Figure 7: Illustration of linear interpolation. Left panel shows all available points from a combination of QMC and NCE data sets. Right panel shows a close up view and the triangulation scheme which is used to linearly interpolate. The value at the red point is determined by the 3 green points which form the triangle that enclose it. Note that the value of $S_{\boldsymbol{\pi}}/n$ at each green point is obtained from the data tables at the local chemical potential of interest.

local chemical potential, the local U/t and the local T/t.

2. Use the NLCE data to find the global chemical potential that produces the desired atom number N. The temperature used simply needs to be $T/t < 1.0$, since $n(\mu)$ is frozen below this temperature.
3. For the local $S_{\boldsymbol{\pi}}/n$ determination, set a value of $[T/t]_0$. This is the local value of T/t at the center of the trap. Use the global chemical potential (from 2) along with the local U/t and T/t to get the local S_{π}/n via interpolation from available QMC and NLCE data.
4. Integrate the local $S_{\boldsymbol{\pi}}/n$ over the trap to obtain the bulk spin structure factor $\bar{S}_{\boldsymbol{\pi}}$.
5. Repeat 3 and 4 for decreasing values of $[T/t]_0$ until the resulting $\bar{S}_{\boldsymbol{\pi}}$ agrees with the experimental measurement.

5.1 Determination of $S_{\boldsymbol{\pi}}/n$ by interpolation

We use a combination of the available QMC and NLCE data set to find out $S_{\boldsymbol{\pi}}/n$ for given local values of μ/t, U/t, and T/t. To allow evaluation for arbitrary values of the parameters we interpolate linearly between the available data points. An example is shown in Fig. 7.

5.2 LDA density profiles with NLCE data, dependence on T

To illustrate the effect of temperature on the density profile we show in Fig. 8 density profiles with $n = 1$ at the center, calculated for various values of $[T/t]_0$, where $[T/t]_0$ is the local value of T/t at the center of the cloud. The sample is assumed to be isothermal so it has constant T throughout, the local value of t varies due to the size of the lattice beams. As expected we see that for $[T/t]_0 < 1$ the density

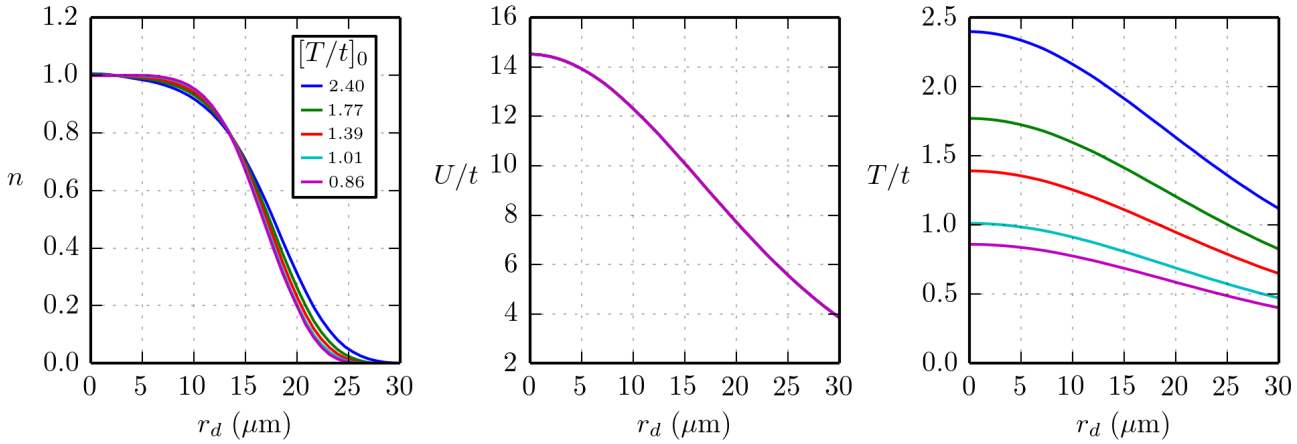

Figure 8: Density profiles with $n = 1$ at the center for various values of $[T/t]_0$. For $[T/t]_0 < 1$ the density profile changes very little with temperature. The right two panes show the spatial variation of U/t and T/t across the sample, illustrating the degree of inhomogeneity in the system.

profile does not change very much, which validates our approach of calculating the density profile and determining the global chemical potential at a single $T/t < 1.0$ using the NLCE data (see step 2 in the prescription outlined above).

5.3 LDA S_π/n profiles, lowest accessible T variation of N

In the experiment we varied the atom number to maximize the Bragg signal for a given value of $[U/t]_0$. Here we calculate S_π profiles for various atom numbers and show how does the bulk spin structure factor $\bar{S}_\pi$ varies with atom number.

The results for the lowest accessible values of $[T/t]_0$ are shown in Figs. 9-12. Even though there is data available down to $T/t = 0.36$ the lowest accesible $[T/t]_0$ is only 0.68 because as one moves radially outwards the local T/t decreases. We are limited by the local value of T/t at the edge of the cloud.

Notice that in Figs. 9-12 we indicate values for $[T/t]^*$ and $[U/t]^*$, which are the local values of T/t and U/t where S_π/n is maximized.

The main features that stand out from Figs. 9-12 are

1. Looking at weak interactions ($[U/t]_0 = 7.6$) we see that the peak in $\bar{S}_\pi$ as a function of N is much broader than what we have observed in the experiment.

2. Looking at strong interactions ($[U/t]_0 \geq 14.5$) we see that $\bar{S}_\pi$ continues to increase with atom number. For larger atom numbers the contribution to the structure factor is coming from the outermost shell of the cloud. We are afraid that our spherical symmetry assumption may not apply as far out from the center and that $\bar{S}_\pi$ should ultimately decay with increasing atom number, as we observe in the experimental data.

5.4 $\bar{S}_\pi$ vs. N for various T's

Finally we repeat calculations like those shown in Figs. 9-12 for several temperatures and show the results for $\bar{S}_\pi$ in Fig. 13. Some comments are included in the figure caption.

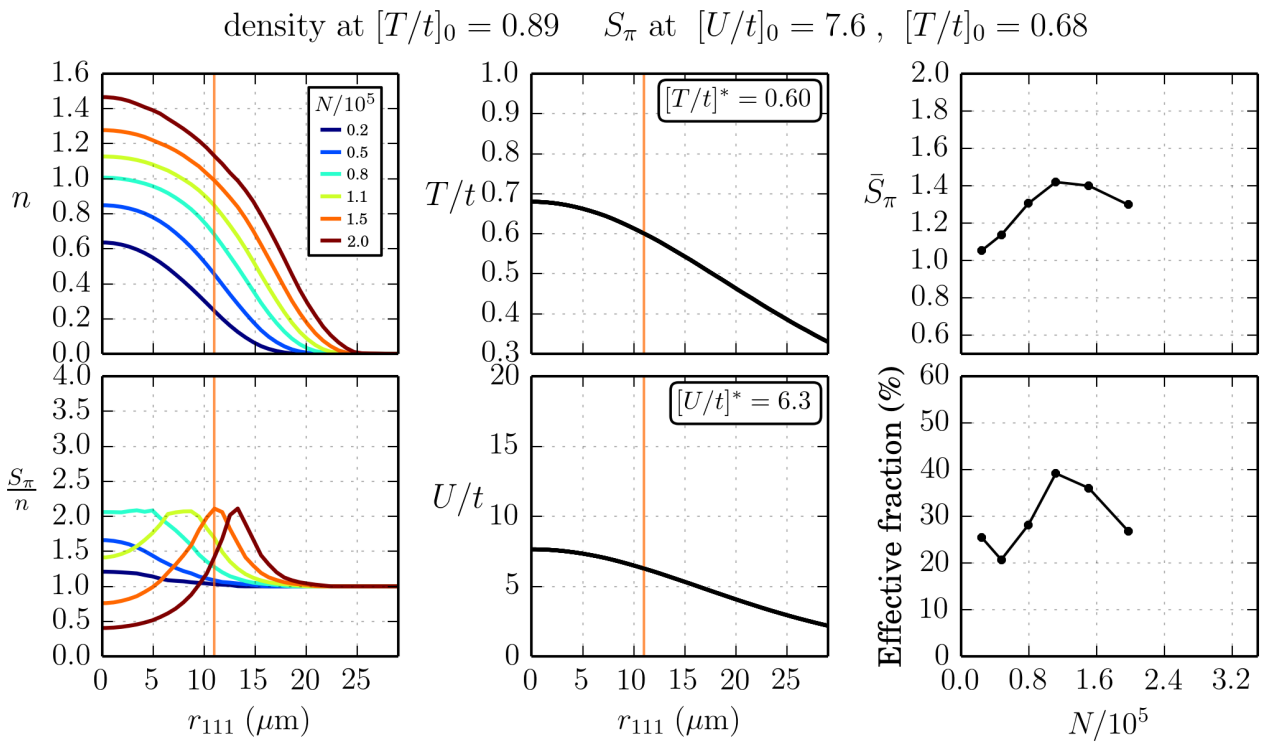

Figure 9: Scattering length $200\,a_0$ ($[U/t]_0 = 7.6$). Variation of density profile, S_π/n profile, $\bar{S}_\pi$ and effective fraction with atom number.

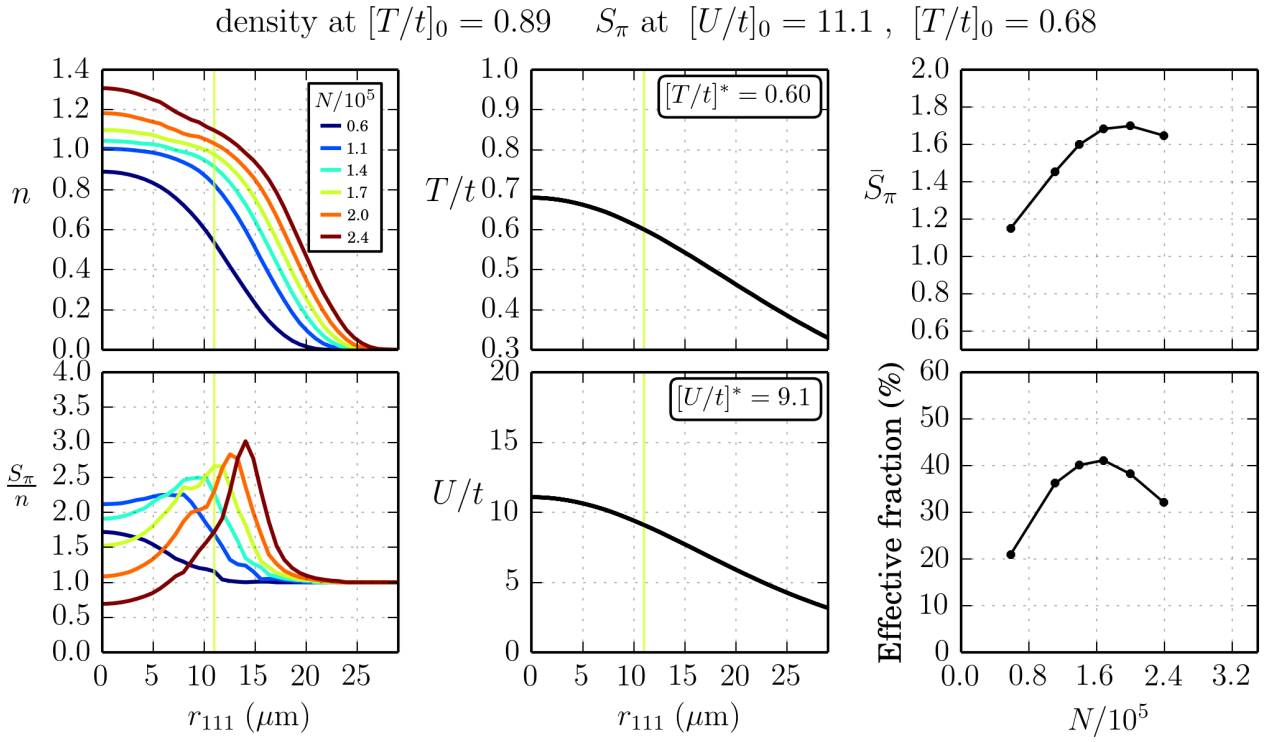

Figure 10: Scattering length $290\,a_0$ ($[U/t]_0 = 11.1$).

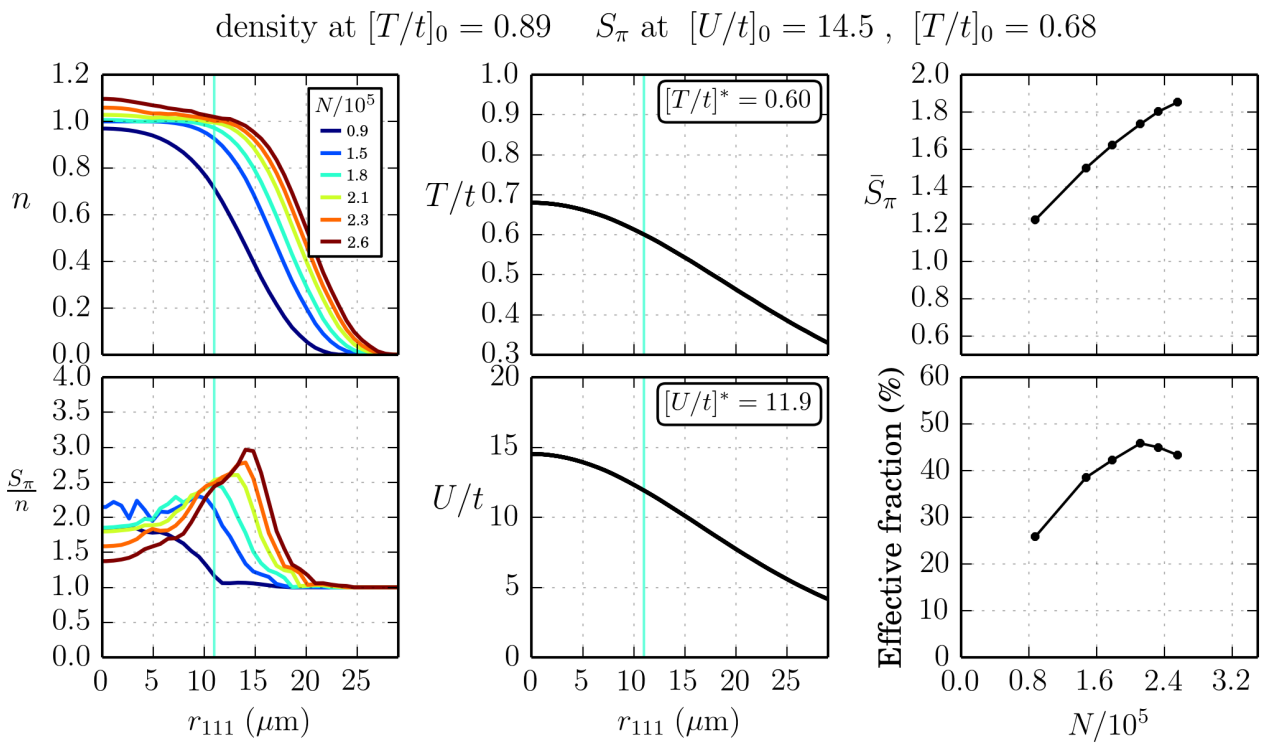

Figure 11: Scattering length $380\,a_0$ ($[U/t]_0 = 14.5$).

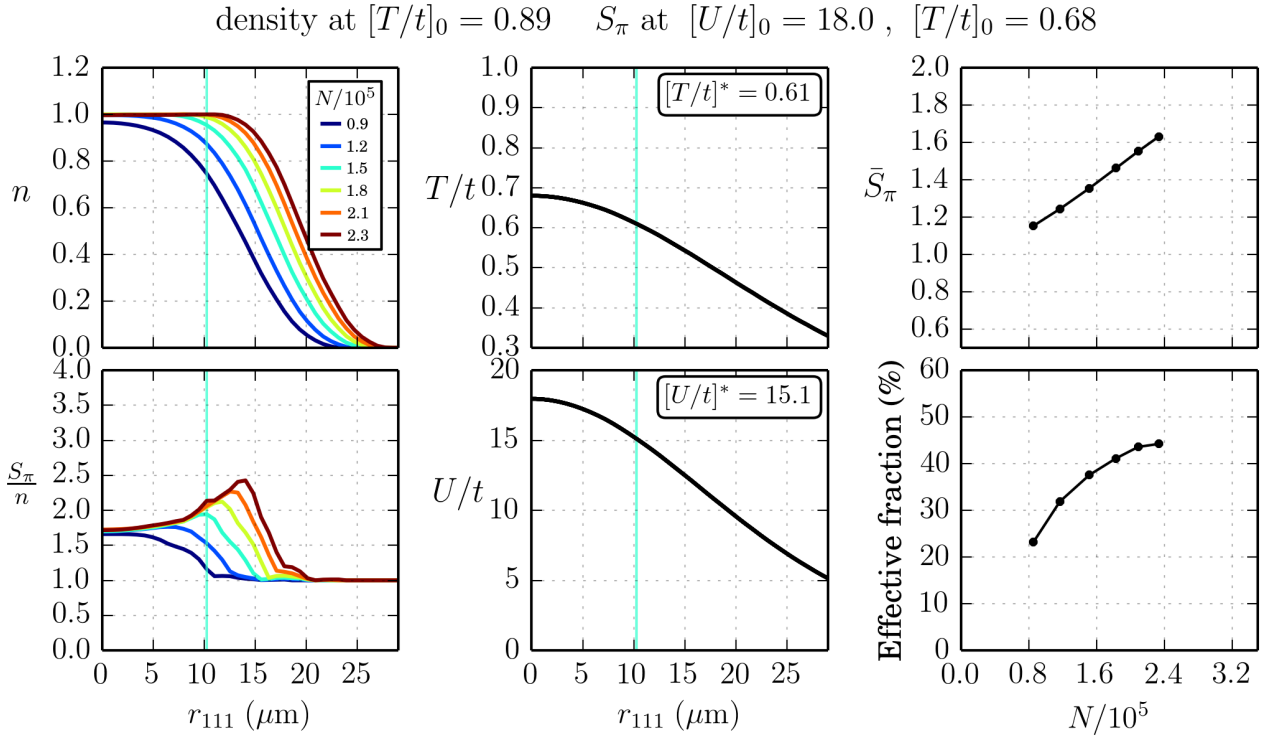

Figure 12: Scattering length $470\,a_0$ ($[U/t]_0 = 18.0$).

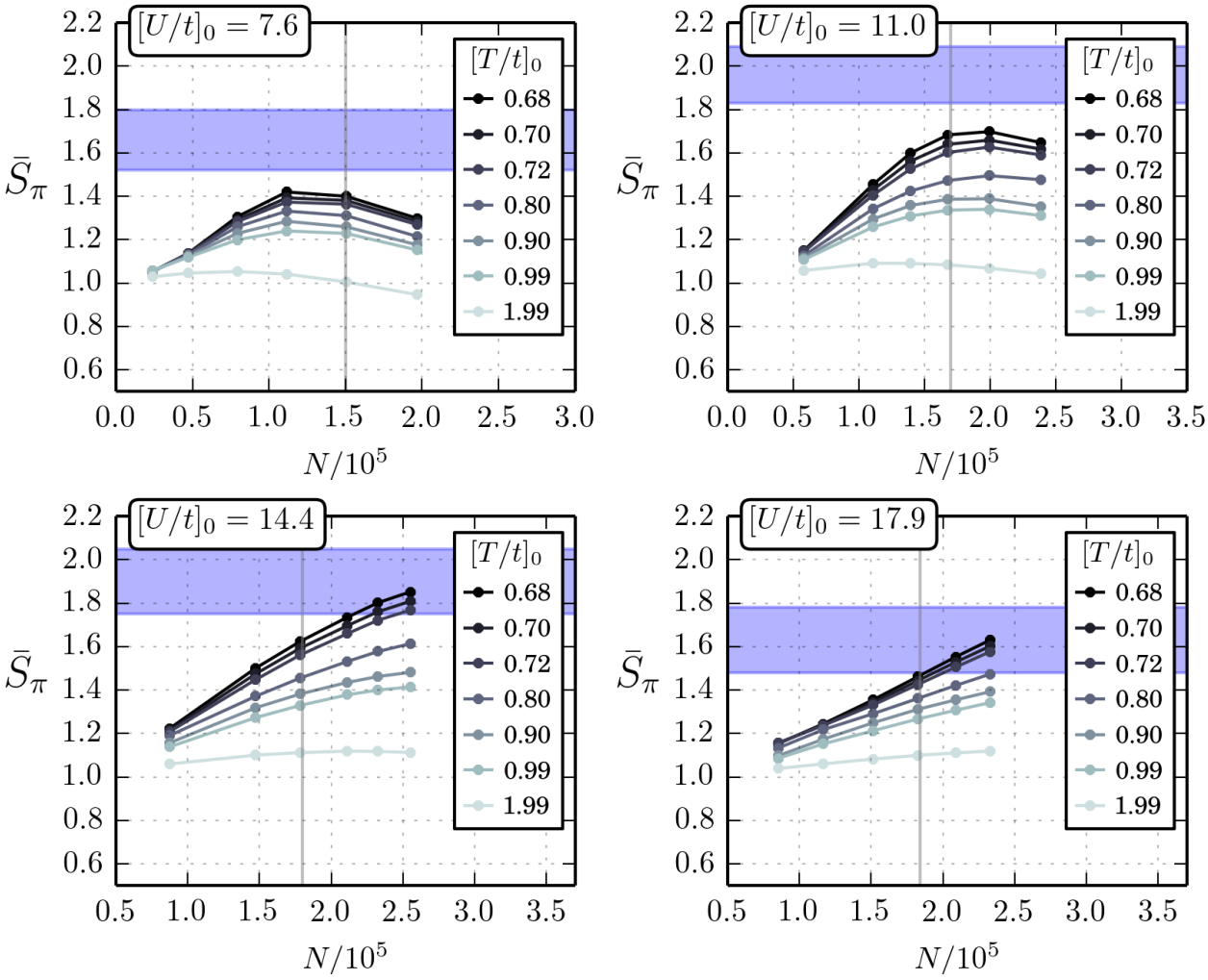

Figure 13: Final comparison of experimental data with LDA. The shaded blue area indicates the experimental range for $\bar{S}_\pi$. The vertical gray line indicates the atom number at which the Bragg signal peaks up in the experiment. For larger atom numbers the spherical symmetry assumed in the LDA comes into question. We see that the lowest temperature accessible at the moment, $[T/t]_0 = 0.68$, is not cold enough to reproduce the $\bar{S}_\pi$ observed in the experiment for $[U/t]_0 \leq 14.4$. In the case of $[U/t]_0 = 17.9$ at the value of N relevant for the experiment (vertical gray line) the LDA at $[T/t]_0 = 0.68$ just touches the experimental error bar.